Impact of the electroforming process on the device stability of epitaxial Fe-doped $SrTiO_3$ resistive switching cells

T. Menke, R. Dittmann, P. Meuffels, K. Szot, and R. Waser

Citation: Journal of Applied Physics **106**, 114507 (2009);
View online: https://doi.org/10.1063/1.3267485
View Table of Contents: http://aip.scitation.org/toc/jap/106/11
Published by the American Institute of Physics

Impact of the electroforming process on the device stability of epitaxial Fe-doped $SrTiO_3$ resistive switching cells

T. Menke,[a] R. Dittmann, P. Meuffels, K. Szot, and R. Waser
Institute of Solid State Research, Forschungszentrum Juelich, 52425 Juelich, Germany

(Received 1 September 2009; accepted 31 October 2009; published online 10 December 2009)

In this work, the results of our detailed investigations on the electroforming procedure in $Pt/SrTi_{0.99}Fe_{0.01}O_3/SrTi_{0.99}Nb_{0.01}O_3$ [Pt/STO(Fe)/Nb:STO] metal-insulator-metal (MIM)-devices and its impact on the performance of resistive switching memory devices are presented. Questions about the exact location of the modifications triggered by the electroforming procedure within the investigated MIM-devices will be addressed. From a technological point of view, the thermal stability of formed devices becomes important. An increase in the device resistances during retention measurements has been observed indicating the presence of internal redistribution effects. These may result from an oxygen vacancy gradient induced by the forming process. However, these internal relaxation effects will not end up in the unformed state. Annealing experiments under defined atmospheric conditions allowed distinguishing between internal and external rediffusion effects. We found that $SrTiO_3$ starts to interact with the surrounding atmosphere at moderate temperatures. The occurring external reoxidation effect set the device back to its initial (unformed) state. As a result, the investigated MIM-structures can no longer be regarded as closed systems and presented the large implication on the retention of such devices. The experimental findings are supported by calculations of the penetration depth of oxygen ions/vacancies in $SrTiO_3$. © *2009 American Institute of Physics*. [doi:10.1063/1.3267485]

I. INTRODUCTION

In order to extend the validity of Moore's law and to overcome the limitations of the present memory technologies in the long run, alternative information storage concepts need to be developed. Since different material classes such as oxides,[1,2] semiconductors,[3] or organic compounds[4] exhibit reversible switching between two or more stable resistive states by applying an appropriate threshold voltage, these materials are under consideration for the use in resistive random access memory (RRAM) devices.

Typically, a forming procedure is needed to "enable" the resistive switching in metal-insulator-metal (MIM) devices. By applying thermal[5] or electrical[6–8] stress, the conductivity of the initially insulating materials can be increased by several orders of magnitude. The "conducting" state after electroforming allows reproducible switching between different impedance states triggered by means of current or voltage pulses.

In the case of oxides, the electroforming process (forming by electrical stress) has been explained by the creation and redistribution of oxygen vacancies.[9] This has been facilitated by the effect of high electric fields and local Joule heating.[10] Changes in the oxygen vacancy concentration bring about changes in the conductivity due to the so-called self-doping effect. Most of the models are based on the assumption that these defects form filamentlike defect structures within the bulk thus locally modifying the bulk conductivity. The created oxygen vacancies will accumulate at the cathode and form a conducting path which proceeds through the oxide toward the anode during the electroforming step.[11]

Within the class of perovskite-type oxides, $SrTiO_3$ can be regarded as a model system.[12–15] The electrical transport properties of $SrTiO_3$ have been intensively studied over several decades and the defect chemistry of this compound seems to be understood in great detail. Thus, $SrTiO_3$ represents a promising material for a further elucidation of the underlying physical effects related to the electroforming and switching mechanisms of perovskite-type oxides. The electrical properties of $SrTiO_3$ (STO) can be modulated from a band insulator to metallic conduction by self-doping with oxygen vacancies which act as shallow donors. A local accumulation or depletion of oxygen vacancies at the vicinity of the STO/electrode interface will lead to local redox processes which are responsible for the resistance switching effects.[16]

Szot *et al.*[17] demonstrated that, using $SrTiO_3$ single crystals, the electroforming process removes oxygen ions from the crystal lattice which becomes evident by the appearance of gas bubbles under the anode. The evolution of oxygen gas bubbles was also observed in thin film $Pt/TiO_2/Pt$ samples by Jeong *et al.*[9] and Yang *et al.*[10]

Conductive atomic force microscopy (*LC*-AFM) measurements performed on $SrTiO_3$ single crystals[17] and epitaxial thin films[18,19] indicated a laterally confined and filamentary current transport within the material. The conducting filaments were attributed to extended defects such as edge dislocations.[17] Thus it can be assumed that even pristine samples exhibit some inhomogeneity with respect to the electrical conductivity due to the existence of these extended defects. This inhomogeneity will be intensified by the electroforming procedure leading to an electrochemical reduction in only a few preferred filaments. A confined current

[a]Electronic mail: t.menke@fz-juelich.de.

transport was also found by Yang *et al.* in formed TiO_2 MIM-devices.[10,20] Furthermore, electron beam induced current measurements[21] on Pt/$SrZrO_3$/SRO structures have also shown that confined conduction paths exist below the metal electrode after the electroforming process. In epitaxial Sr_2TiO_4 thin films, Shibuya *et al.*[22] found another type of forming process which exhibits a "homogeneous" character and can be explained by a homogeneous distribution of the conducting filaments beneath the electrode.

In this publication, we will present the results of our detailed investigations of the forming procedure of MIM-devices, made of epitaxially grown Fe-doped $SrTiO_3$ [STO(Fe)] thin films as the "switching" layers and Pt and Nb-doped $SrTiO_3$ (Nb:STO) as electrode materials. In view of a technological application, questions such as the thermal stability of the formed device or a possible gas exchange during the electroforming process will become of fundamental interest and will be discussed in detail. In addition, the experimental findings are supported by calculations of the penetration depth of oxygen ions/vacancies in $SrTiO_3$. The entireness of the results allows an interpretation of the retention behavior of formed MIM-devices which is high important with respect to a nonvolatile memory application.

II. EXPERIMENTAL DETAILS

Epitaxial, nominally 1 at. % STO(Fe) thin films with thicknesses between 45 nm and 750 nm were grown by pulsed laser deposition using a KrF excimer laser ($\lambda = 248$ nm) and a ceramic $SrTi_{0.99}Fe_{0.01}O_3$ target. Single crystalline Nb:STO was used as substrates. The deposition parameters were chosen to a laser energy density of 1.55 J/cm^2, a deposition temperature of 700 °C, an oxygen partial pressure of 0.25 mbar and a repetition rate of 5 Hz. After the deposition process, the samples were cooled down in an oxygen atmosphere of 500 mbar. The deposited films were characterized by x-ray diffraction to confirm the epitaxial growth. The surface roughness (rms) was smaller than 0.5 nm as found by AFM measurements.

To complete the MIM-structure, 100 nm thick Pt top electrodes were deposited by magnetron sputtering and patterned on the one hand by optical lithography and a dry etching process or on the other hand by a shadow mask process to form electrodes with 200 μm diameter. An Ohmic contact to the Nb:STO bottom electrode was achieved by Al wire bonding after removing the STO(Fe) film at a corner of the substrate by a wet etching step using a buffered HF solution.

The current voltage characteristics were measured using a Keithley 2611A source meter by applying the voltage to the top electrode. Impedance spectroscopy was performed in the frequency range 0.01 Hz–3 MHz using a Solatron impedance analyzer (1260 Impedance Gain Phase Analyzer) in combination with a Solatron preamplifier (Dielectric Interface 1296). All impedance measurements were taken at 50 mV_{rms}.

III. LOCATION OF ELECTROFORMING

To investigate the influence of different top metal contacts on the $I(V)$-characteristic a 45 nm thin STO(Fe) film was grown on a (100)-oriented Nb:STO substrate. For the comparison of a deep and a shallow work function metal as the top electrode material, the sample was split after the PLD process. One half was prepared with sputtered electrodes made of Pt which exhibits a work function of 5.65 eV.[23] For the other half, a shallow work function metal — in this case Ti(ϕ_m:4.3 eV)[23] — was chosen. From the simple Mott–Schottky relation ($\phi_{barrier} = \phi_{metal} - \chi_{semiconductor}$) one expects a significantly different electrical behavior for both metal-insulator contacts. For the Ti top electrode, an almost symmetric $I(V)$-curve is found. The device exhibits an — for an insulator — extremely low resistance $<100\ \Omega$ which demonstrates the Ohmic nature of both the Ti/STO(Fe) and the STO(Fe)/Nb:STO interface. Beside the work function, the chemical interaction between the oxidizable Ti and the STO(Fe) in the vicinity of the interface might, by the local reduction in the STO(Fe), support the Ohmic-like behavior of this contact. In comparison, in case of the Pt top electrode, a highly asymmetric characteristic with a significantly higher device resistance is found. The rectifying properties confirm the expected formation of a Schottky barrier at the Pt/STO(Fe) interface which shows, biased in forward direction (Pt positive), the typical exponential $I(V)$-behavior.

Even though the last few monolayer of the STO(Fe) film might show some deviations from stoichiometry due to kinetic demixing by the Pt deposition,[24] we will discuss the properties of this junction by means of the Schottky model. It cannot be excluded that the depletion layer may also result from a Bardeen barrier due to a high concentration of surface states. This, however, would not change our principal conclusions.

Furthermore, we can conclude from the results of both samples that the STO(Fe) films exhibit a significant n-type conductivity at room temperature (RT) which we attribute to the self-doping by oxygen vacancies formed during the deposition.

For the electroformation study Pt/STO(Fe)/Nb:STO devices with STO(Fe) thicknesses of more than 300 nm were investigated. The large film thicknesses allow on the one hand a better comparability to single crystal data and on the other hand the use of impedance spectroscopy to separate between miscellaneous contributions to the device resistance.

Unlike to samples with a low initial resistance which typically do not need a stressing dc-forming treatment,[25,26] the investigated devices with Pt electrodes require an electroforming step to set the sample to a low resistance state.

A typical $I(t)$-forming trace of a device with a STO(Fe) thickness of 750 nm can be seen in Fig. 1. The junction was biased with +10 V at the Pt electrode, corresponding to the forward direction of the Pt/STO(Fe) Schottky contact. During the first 25 s the current remains in the subnanoampere regime and increases just slightly and smoothly with time. After this initial period, spikelike fluctuations of the current appear. These resistance fluctuations can be attributed to the competing reduction and reoxidation in filament fragments

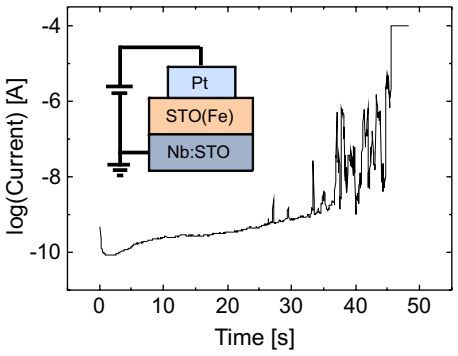

FIG. 1. (Color online) Current vs time curve of a Pt/750 nm STO(Fe)/Nb:STO junction by applying +10 V to the Pt top electrode.

within one or more conducting filaments that are growing during the electroforming process.[17] After a certain time, in case of the sample shown in Fig. 1 after 45 s, a steep increase in the current occurs and the current compliance is attained. The compliance was set to 100 μA to prevent dielectric breakdown. The forming process was stopped as soon as the current reached the compliance due to the fact that bipolar switching can be observed at this stage.

By applying a positive voltage to the top electrode oxygen ions migrate toward the top interface get oxidized and are released to the surrounding. By biasing the junction with opposite polarity [Pt(−)], corresponding to the reverse direction of the Schottky contact, no degradation could be observed. This finding is different to, e.g., $Pt/TiO_2/Pt$ devices which can be formed with different polarities.[9,10] It is well known from point defect chemistry arguments[27,28] that Nb:STO, i.e., n-conducting donor doped STO, exhibits a negligible amount of oxygen vacancies under normal conditions. Thus, Nb:STO cannot really act as a sink for oxygen ions so that the forming process does not work in the opposite [Pt(−)] direction.

A. Filamentary versus homogeneous effect

In addition to the laterally confined current transport found by *LC*-AFM investigations in STO,[17–19] we found that even in our pristine STO(Fe) films there exist filamentlike defect structures which differ in conductivity from the surrounding. *LC*-AFM measurements performed on our STO(Fe) thin films (see Fig. 2) showed in addition to the small conducting filaments [Fig. 2(c)] a strong inhomogeneity of the conductance on a larger scale (>100 nm) [Fig. 2(b)]. This broad pattern of conducting regions is attributed to a clustering of single filaments. These findings underline the strong influence of the filament distribution on the electrical properties of the investigated thin films.

To investigate the lateral expansion of the transformation triggered by the forming process within MIM-structures, a Pt/500 nm STO(Fe)/Nb:STO stack was prepared and structured to MIM-junctions with top electrode diameters of 200 μm. Two top electrodes were connected using wire bonding with a thin Al wire. After connecting the two top electrodes, a probe tip was used to bias the whole "segmented" top electrode against the bottom electrode. Impedance measurements were performed before and after the

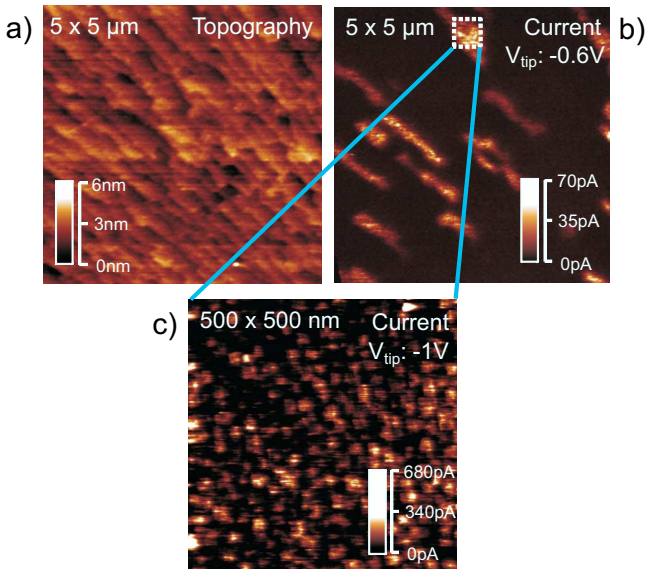

FIG. 2. (Color online) *LC*-AFM images of a 200 nm thin STO(Fe) film recorded under vacuum conditions. (a) Topography image of a 5×5 μm^2 scan. (b) The corresponding current image. (c) Current image of a 500×500 nm^2 scan.

forming process to determine the resistance of the junction. The electrical configuration during the forming process is shown in Fig. 3(a). In the lower part of the figure, the frequency dependence of the real part, Z', of the complex impedance before and after the degradation can be seen. By fitting these data the dc resistance $R_{dc}(\omega->0$ Hz) can be determined. Before applying electrical stress, the junction resistance is more than 10 GΩ, after the forming process a decrease by a factor of nearly 10^5 to a R_{dc} value of 3 MΩ was measured.

Afterwards, the connection between the two Pt pads was cut and the resistance of each part was measured against the bottom electrode. As exhibited in Fig. 3(b), the resulting R_{dc} obviously varies for both pads. One pad shows a huge resistance in the GΩ-range which is comparable to the value determined for the unformed state of the connected junctions. The other pad reveals a R_{dc} of 3 MΩ which is equal to the value determined for the connected junctions after forming. This is a strong indication that the electroforming pro-

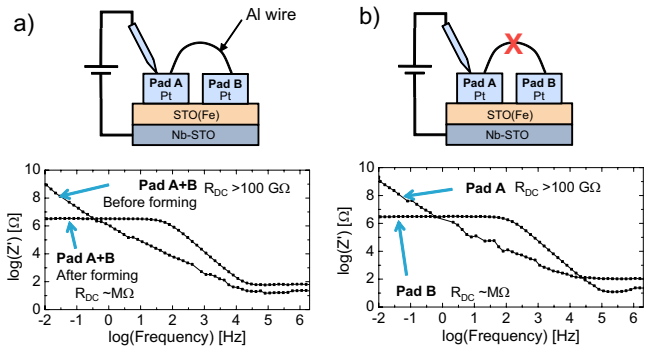

FIG. 3. (Color online) Electroformation of a segmented electrode on a 500 nm thick STO(Fe) film (V_{form}=+5 V). The Bode plots of Re(Z), Z', shown in (a) represent the properties of the connected pads before and after the forming procedure. Part (b) displays Re(Z) for each pad after breaking up the connection.

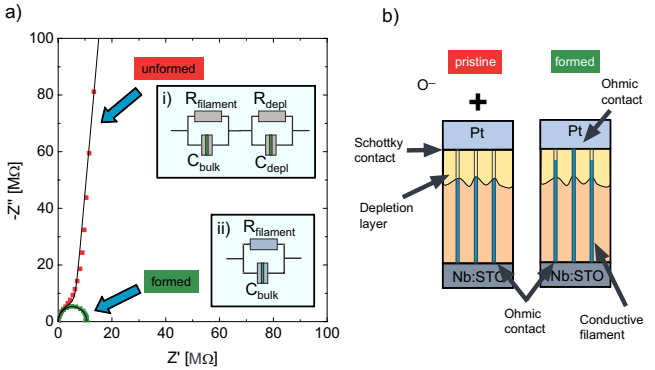

FIG. 4. (Color online) (a) Impedance spectra of a Pt/750 nm STO(Fe)/Nb:STO MIM-structure before and after a dc-forming process. The equivalent circuits used for fitting are displayed in the inset for (i) the unformed case with $R_{filament}$=7.3 MΩ, C_{bulk}=277 pF, R_{depl}=17.9 GΩ, and C_{depl}=914 pF and for (ii) the formed case with $R_{filament}$=10.7 MΩ and C_{bulk}=273 pF. (b) Model for the electroforming process and the local bypassing of the Schottky depletion layer.

cess is a local phenomenon, e.g., due to the formation of a conducting filament. These findings are consistent with results found in TiO_2 devices by Jeong *et al.*[9] and Yang *et al.*[20]

B. Bulk versus interface effect

The impedance spectrum of a Pt/750 nm STO(Fe)/Nb:STO sample in the pristine, unformed state, was measured. Since the thickness of the STO(Fe) film is larger than the depletion layer width, which was determined by $C(V)$ measurements to be about 200 nm, two contributions to the complex impedance are expected.[29] The corresponding Cole–Cole plot and the equivalent circuit which is proposed to fit the data are shown in Fig. 4 and in the inset (i), respectively. The series inductance of the leads as well as the series resistance of the Nb:STO bottom electrode was taken into account for fitting the equivalent circuit models but is not depicted in the diagrams. The impedance spectra of the STO(Fe) film can be perfectly described by two Voigt elements resulting from the bulk and the depletion layer properties.

Due to the confined character of the electrical properties, the resistance of the bulk related contribution to the impedance will be dominated by the conducting filaments.[29] Furthermore, to pay tribute to the inhomogeneity of the electrical properties found by *LC*-AFM measurements the impedance spectra were described by the use of a constant phase element within the Voigt element.

The impedance analysis implies that the overall resistance in the unformed state is dominated by the depletion layer resulting from the Schottky contact at the Pt/STO(Fe) interface. To electroform the device, a dc voltage of +10 V was applied to the Pt electrode, corresponding to the forward direction of the Schottky contact. The result of the impedance measurements on the formed sample can be seen in Fig. 4 and can be described using the equivalent circuit displayed in the inset (ii). The most significant change in the spectrum of a formed sample is that only one Voigt element is needed to fit the data. As the values for the resistance and the capacitance are comparable to the values obtained for the bulk related Voigt element in the unformed state, the Voigt element can be attributed to the bulk contribution. Thus we can conclude that the electroforming procedure leads to a local bypassing of the Schottky depletion layer. It is reasonable to assume that this local bypassing takes predominately place in regions with clustered filaments. The bypass of the depletion layer on areas larger than approximately $\varnothing 100$ nm will furthermore explain the fully elimination of the depletion layer contribution to the impedance spectrum in the formed case.

C. Model for the electroforming process

By applying a positive voltage to the top electrode oxygen ions migrate along extended defects toward the top interface and are released to the surrounding.[17] In contrast to STO single crystals, where a virtual cathode moves toward the anode until a conductive path is established during the forming procedure,[11] the present as-deposited thin films already contain so to speak "preformed" conducting paths along extended defect structures as a result of the reducing deposition conditions. Since the overall resistance in the unformed case is dominated by the depletion layer, most of the applied voltage drops in the vicinity of the top interface. Taking into account that the movement of oxygen ions is a field-driven process, one can conclude that the electroforming process most likely removes oxygen directly next to the top interface where the electrical field is strongly enhanced.

Due to the donor character of oxygen vacancies, a significant reduction in the effective Schottky barrier height and of the depletion layer width at the Pt/STO(Fe) interface can be expected. *Ab initio* calculations predict that the creation of oxygen vacancies will create additional states within the bandgap next to the bottom of the conduction band.[17,30] The resulting shift in the Fermi level can lead to an insulator/metal transition under strong reducing conditions. Under ambient conditions, the electroformation usually leads to a highly donor doped STO system with a thermally activated current.

The different work functions of Pt and STO [$\phi_{STO} = \chi_{STO} - (E_{CB} - E_F) < \phi_{Pt}$] will lead to a Schottky contact and therewith to a space charge layer within the STO. The width of this space charge region (or depletion region) strongly depends on the doping concentration. Since the electroformation increases the doping level, the width of the depletion layer shrinks dramatically. For thin depletion layers, charge carriers can be injected from the semiconductor to the metal or vice versa by quantum mechanical tunneling through the potential barrier instead of by a thermionic emission process. It is well known that the tunneling based injection mechanism is responsible for most Ohmic contacts. The transition of a Schottky contact to an Ohmic contact is in agreement with the voltage-induced elimination of the Schottky barrier observed at the interface between Pt electrodes and TiO_2 single crystal.[31]

Localized bypassing of the Schottky depletion layer can explain that the depletion layer contribution to the impedance disappears and that the bulk properties are not significantly changed during the forming procedure. To confirm this statement reference samples with Ti top electrodes

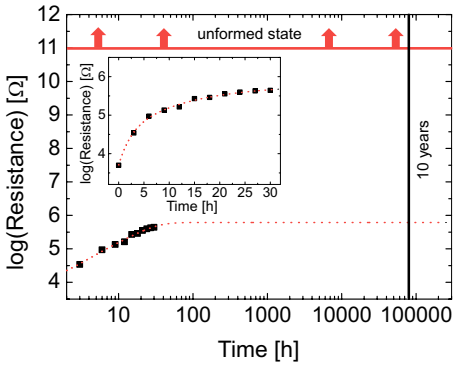

FIG. 5. (Color online) The time dependence of the resistance of a Pt/500 nm STO(Fe)/Nb:STO device recorded after the electroforming step (line: guide to the eyes).

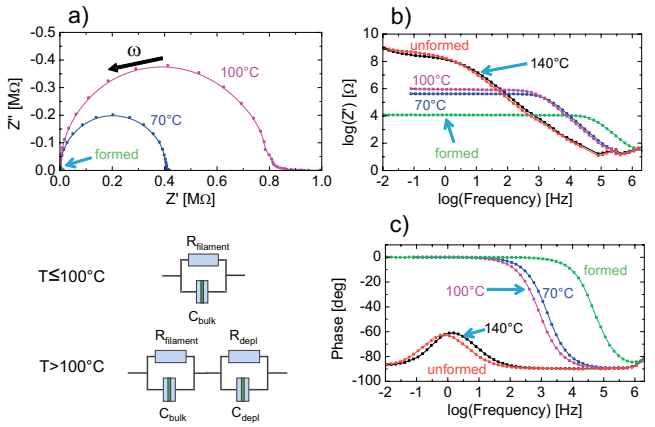

FIG. 6. (Color online) (a) Cole–Cole plots of Pt/500 nm STO(Fe)/Nb:STO at different temperatures after an initial forming at RT; [(b) and (c)] The corresponding Bode plots of Z' and the phase.

which provide an Ohmic contact were prepared. As expected, the impedance spectra exhibited only the bulk contribution. A much shorter, or for some devices, even no electroforming process was necessary to achieve bipolar resistive switching.

IV. STABILITY OF FORMED STATE

A. Retention of the formed state

For this study, samples with a STO(Fe) thickness of 500 nm with Pt top electrodes and Nb:STO bottom electrodes were used. All MIM-devices underwent a forming procedure, as described above, to set them to the low resistive state (LRS). Afterwards, the frequency dependent impedance was measured resulting in spectra originating only from the bulk contribution. The formed samples were stored at RT and under ambient gas atmosphere for 30 h. During that time an impedance spectrum was periodically taken every three hours.

The resulting Cole–Cole plots can be fitted in particular by only one Voigt element. For all spectra, the capacitance could the determined to be 280 pF without any time dependence. However, the resistance of 5 kΩ immediately after forming clearly increased by nearly two orders of magnitude during 30 h. The time dependence of the resistance is plotted in Fig. 5. The clear slowdown of the resistance drift with time is obvious (see inset of Fig. 5).

To explain this drift we have to keep in mind that during the electroforming procedure a chemical gradient in the oxygen vacancy concentration was induced which is supposed to partly re-equilibrate after releasing the electrical stress. Due to the slowdown of the resistance drift and the absence of the depletion layer contribution the drift may be attributed to an internal relaxation/redistribution of oxygen ions/vacancies. A simple fit based on the data points and its extrapolation toward the 10 year mark specified for nonvolatile RRAM (dotted line in Fig. 5) indicated that the resistance will not drift to the value found before forming. We identify this relaxation as a pure internal effect because an external effect (reoxidation from the surrounding atmosphere) would cause to the total recovery of the initial/unformed state.

In the first view, this drift makes it unlikely to use this material for a memory device. However, the resistance drift toward larger values will finally not lead to the high resistive state (HRS). In addition, the drift can be avoided by the use of samples with thinner films which typically need only a short or no forming process.[10,25,26]

Furthermore, it has to be mentioned that only small resistance drifts were observed for devices which were subsequently switched after the forming treatment to the HRS or LRS, respectively (not shown here). This can be understood by regarding the oxygen gradients induced by the two different processes (electroforming and resistive switching). The electroforming induces, as a result of the large bias applied, a strong chemical gradient within the device which afterwards starts to relax partially over time. In contrast, the resistive switching will only induce small changes in the oxygen concentration next to the interfaces[16] so that strong relaxation effects will not occur.

B. Thermal stability of the formed state

Since the drift of the resistance at RT seems to be an internal process, annealing experiments were performed to clarify at which temperature an oxygen exchange with the surrounding atmosphere is observed. Therefore, a formed sample was subjected to some moderate thermal stress. The frequency dependent impedance was measured at temperatures between RT and 140 °C, starting at RT. A time delay of 20 min was kept for each temperature to set the sample into thermal equilibrium.

The results of the impedance study are displayed in Fig. 6 in terms of Cole–Cole plots [Fig. 6(a)] and Bode plots of Z' [Fig. 6(b)] and the phase [Fig. 6(c)], respectively. The spectra taken at RT and at 70 °C can be fitted with one Voigt element and can be related to the bulk properties as described above. Since the electrical conduction of STO is thermally activated, the resistance should decrease with increasing temperature which is, however, not the case. Instead, an increase from 10 kΩ at RT to 400 kΩ at 70 °C has been determined and can be attributed to an internal redistribution of oxygen ion/vacancies such as in the previous experiment. Since no drift of the resistance during the measurement (duration around 20 min) at 70 °C was detected it seems that the sample had achieved its equilibrium state. Looking now at

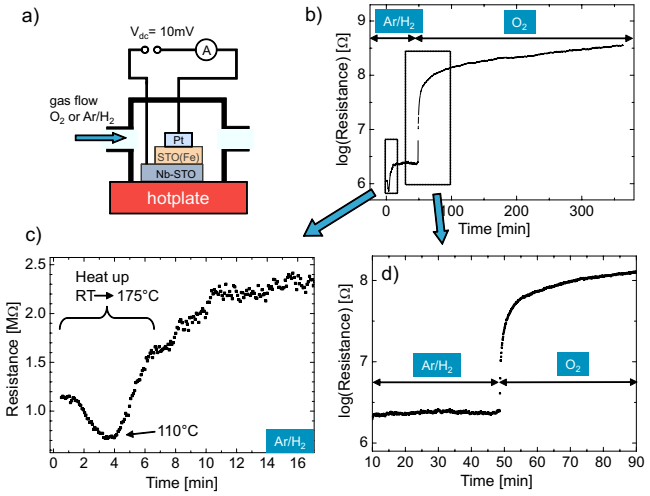

FIG. 7. (Color online) (a) Sketch of the setup used to study the influence of the oxygen partial pressure on a formed Pt/500 nm STO(Fe)/Nb:STO stack at 175 °C. The device resistance plotted as a function of time can be found in part (b), (c), and (d).

the Cole–Cole spectrum taken at 100 °C, an increase in the device resistance by a factor of two is found. In contrast to the measurement performed at 70 °C, the 100 °C spectrum indicates that, because of the abnormal drift of Z' at low frequencies [see Cole–Cole plot in Fig. 6(a)], the sample has not achieved a stable state. The assumption that an internal re-equilibration should proceed faster at elevated temperatures indicates that an additional mechanism at 100 °C shows up. A further increase in the temperature to 140 °C led to a drastic increase in this effect in which the device resistance (at $\omega->0$ Hz) changes from the sub-megohm range to a resistance beyond 10 GΩ. This huge increase was accompanied by the appearance of an additional contribution to the impedance. This becomes most obvious by the frequency dependence of the impedance phase [e.g., Fig. 6(c)].

Measurements at temperatures below 100 °C reveal only one relaxation step in the frequency dependent phase. However, the spectrum taken at 140 °C reveals an additional relaxation step which can be attributed to the total recovery of the depletion layer. A comparison of the 140 °C spectrum with the spectrum of the unformed device strongly supports the idea of a thermal recovery of the Schottky depletion layer. Subsequently we studied whether this recovery originates from an internal redistribution and/or a reoxidation from the surrounding atmosphere.

C. Oxygen partial pressure dependence

A typical MIM-structure consisting of a 500 nm thin STO(Fe) layer was electroformed in the described way. As is sketched in Fig. 7(a), the sample was mounted on a hotplate within a chamber. The gas atmosphere in the chamber could be adjusted by applying a constant gas flow of Ar/H_2 or O_2, respectively. The resistance of the device was measured by applying $V_{dc}=10$ mV and recorded as a function of time.

Heating up of the sample from RT to 175 °C was done under a reducing atmosphere of Ar/H_2. Before starting the experiment, the chamber was purged with Ar/H_2 for 1 h. The recorded resistance can be seen in Fig. 7(c). After the forming procedure the device resistance was about 1.15 MΩ and decreased within the first 4 min during the heat up. This is typical for a thermally activated conduction. However, when the temperature exceeded 110 °C (after ~4 min) the resistance increased with time to approx. 2.3 MΩ. Since no oxygen is supported from the reducing atmosphere an internal redistribution must be the origin for the resistance increase.

Since the mobility of oxygen vacancies increases exponentially with the temperature the fast relaxation (several minutes) at 175 °C will be attributed to the same relaxation effect that was found at RT as shown in Fig. 5 (several hours). Due to the fact that the forming procedure for this annealed sample was stopped before a complete degradation took place, the initial resistance was larger compared to a completely formed device. Therewith, the internal redistribution does not show the same dramatic influence on the resistance.

After the internal gradient in oxygen vacancy concentration was reduced, the sample reached a steady state. At this stage (ca. 50 min) the gas atmosphere was changed from Ar/H_2 to O_2. Figure 7(c) displays the resistance recorded during the gas change. Under Ar/H_2 atmosphere the device resistance at 175 °C was determined to be 2.3 MΩ and showed no time dependence. The exchange of the gas atmosphere ($Ar/H_2->O_2$) resulted in a drastic increase in the resistance by nearly two orders of magnitude within a few minutes. Furthermore, a slower steady increase in the resistance over the whole recorded time (5 h) was recorded as can be seen in Fig. 7(b).

This strong influence of oxygen on the device resistance shows that the Pt/STO(Fe)/Nb:STO device allows for a gas exchange with the surrounding atmosphere at 175 °C. Additionally, the result supports the view that electroforming removes oxygen from the $SrTiO_3$. It has been already reported that oxygen diffuses along Pt grain boundaries even at RT.[9,32] Consequently, the reoxidation of the MIM-structure preferentially takes place at the upper interface and will, therefore, lead at the beginning to an increased oxygen content below the Pt electrode thus restoring the Schottky depletion layer. Since the overall resistance of a Pt/STO(Fe)/Nb:STO device is dominated by the Schottky depletion layer the fast increase in the resistance can be attributed to this effect. The slower increase after longer times seem thus to result from reoxidation effects occurring deeper inside the STO layer.

D. Simulation results

Since $SrTiO_3$ is well studied in terms of point defect chemistry, the activation energy for the diffusion of oxygen vacancies is known.[11,33–35] The experimentally determined values of the activation energy vary between 0.86 and 1.005 eV.

An extrapolation of the high-temperature values to lower temperatures allows a calculation of the chemical diffusion of oxygen within $SrTiO_3$ by using Fick's second law (one-dimensional case). As sketched in Fig. 8(a), the concentration of oxygen vacancies is calculated at several points along the x axis corresponding to the depths within the STO layer. An infinite reservoir of oxygen at $x=0$ and a constant amount

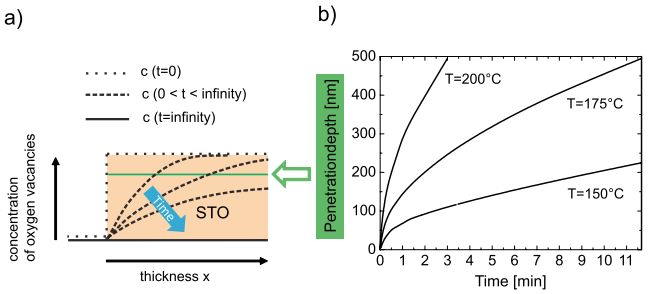

FIG. 8. (Color online) (a) Sketch of the calculated oxygen vacancy distribution. (b) Calculated penetration depth of oxygen within a $SrTiO_3$ single crystal for different temperatures.

of oxygen vacancies within the STO were chosen as starting values. According to the annealing experiment, a 500 nm STO layer at 175 °C was simulated (parameters used: $E_a = 1.005$ eV, $\mu(V_{\ddot{o}}) = 1.10 \times 10^{-14}$ $m^2\ V^{-1}\ s^{-1}$, $D(V_{\ddot{o}}) = 2.13 \times 10^{-16}$ $m^2\ s^{-1}$ at T=448 K). From the resulting oxygen vacancy distribution a penetration depth for oxygen can be deduced. The penetration depth is defined as the depth where the initial concentration falls to 1/e (ca. 37%) and is plotted against time in Fig. 8(b) for different temperatures.

The chemical diffusion coefficient, $D(\delta)$, describes the diffusion of neutral components, and, for ionic compounds, a charge-neutral ambipolar diffusion of at least two chemically different charged defects, e.g., $V_{\ddot{o}}$ and e'. The chemical diffusion coefficient depends in complex way on the ionic and electronic defect diffusivities. Note that the self diffusion coefficient $D(V_{\ddot{o}})$ can be regarded as the lower limit for the considered case of chemical diffusion of oxygen in STO $[D(V_{\ddot{o}}) < D(\delta) < D(h/e')]$[36] and that in nonideal systems the diffusion coefficient exhibits a much more complicated behavior.[37]

However, this plot clearly shows that oxygen can diffuse at 175 °C through 500 nm STO within several minutes. For this estimation the slow ionic diffusion coefficient and no fast diffusion paths, such as extended defects, were taken into account. Furthermore, the highest activation energy, which was found in literature ($E_a = 1.005$ eV) for the hopping transport of oxygen vacancies was used for the calculation. Thus, the resulting values can be regarded as the lower limit for the ion migration. As a result, this calculation represents the "worst-case" scenario for the reoxidation.

Regarding the oxygen triggered resistance increase as measured in the previous experiment [see Fig. 7(d)] and the calculated penetration depths of oxygen ions in STO it becomes clear that both effects show up on the same time scale (several minutes). This validates the assumption of a reoxidation of the thin film sample investigated in the previous experiment.

V. SUMMARY

The electroforming phenomena have been studied on Pt/STO(Fe)/Nb:STO MIM-devices. Using a segmented electrode configuration, it has been shown that these MIM-devices exhibit a laterally confined conduction after an electroforming process. The impact of the electroforming procedure on the impedance spectra of a MIM-device has been investigated. As a result of the highly oxygen deficient films used, the electroforming leads to a local bypassing of the Pt/STO(Fe) Schottky depletion layer. Devices with Ohmic contacts did not need a stressing or even no forming process.

In addition, formed devices were treated by annealing experiments performed under defined atmospheric conditions. *Internal* ion redistributions as well as *external* effects show up independently at elevated temperatures (RT to 175 °C). As the external effect, $SrTiO_3$ starts to interact with the surrounding atmosphere at temperatures higher than 110 °C and, hence, the corresponding MIM cells can no longer be regarded as closed systems at these temperatures. The results of the reoxidation experiments can be regarded as a further support of the view that the electroforming process removes oxygen from the STO layer.

ACKNOWLEDGMENTS

We thank R. Münstermann, M. Waters, K. Shibuya, and R. Bruchhaus for helpful discussion and the critical reading of the manuscript. This work was financially supported by Intel Corp., Santa Clara.

[1] W. R. Hiatt and T. W. Hickmott, Appl. Phys. Lett. **6**, 106 (1965).
[2] A. Beck, J. G. Bednorz, C. Gerber, C. Rossel, and D. Widmer, Appl. Phys. Lett. **77**, 139 (2000).
[3] P. W. M. Blom, R. M. Wolf, J. F. M. Cillessen, and M. P. C. M. Krijn, Phys. Rev. Lett. **73**, 2107 (1994).
[4] E. Lörtscher, J. W. Ciszek, J. Tour, and H. Riel, Small **2**, 973 (2006).
[5] K. Szot, W. Speier, R. Carius, U. Zastrow, and W. Beyer, Phys. Rev. Lett. **88**, 075508 (2002).
[6] S. Karg, G. I. Meijer, D. Widmer, and J. G. Bednorz, Appl. Phys. Lett. **89**, 072106 (2006).
[7] M. Janousch, G. I. Meijer, U. Staub, B. Delley, S. F. Karg, and B. P. Andreasson, Adv. Mater. **19**, 2232 (2007).
[8] B. P. Andreasson, M. Janousch, U. Staub, and I. G. Meijer, Appl. Phys. Lett. **94**, 013513 (2009).
[9] D. S. Jeong, H. Schroeder, U. Breuer, and R. Waser, J. Appl. Phys. **104**, 123716(8) (2008).
[10] J. J. Yang, F. Miao, M. D. Pickett, D. A. A. Ohlberg, D. R. Stewart, C. N. Lau, and R. S. Williams, Nanotechnology **20**, 215201 (2009).
[11] T. Baiatu, R. Waser, and K. H. Hardtl, J. Am. Ceram. Soc. **73**, 1663 (1990).
[12] R. A. de Souza, J. Fleig, R. Merkle, and J. Maier, Z. Metallk. **94**, 218 (2003).
[13] R. Merkle and J. Maier, Angew. Chem. **47**, 3874 (2008).
[14] R. Waser, J. Am. Ceram. Soc. **74**, 1934 (1991).
[15] T. Bieger, J. Maier, and R. Waser, Sens. Actuators B **7**, 763 (1992).
[16] R. Waser, R. Dittmann, G. Staikov, and K. Szot, Adv. Mater. **21**, 2632 (2009).
[17] K. Szot, W. Speier, G. Bihlmayer, and R. Waser, Nature Mater. **5**, 312 (2006).
[18] R. Muenstermann, R. Dittmann, K. Szot, S. Mi, C.-L. Jia, P. Meuffels, and R. Waser, Appl. Phys. Lett. **93**, 023110 (2008).
[19] K. Szot, R. Dittmann, W. Speier, and R. Waser, Phys. Status Solidi (RRL) **1**, R86 (2007).
[20] J. J. Yang, M. D. Pickett, X. Li, D. A. A. Ohlberg, D. R. Stewart, and R. S. Williams, Nat. Nanotechnol. **3**, 429 (2008).
[21] C. Rossel, G. I. Meijer, D. Bremaud, and D. Widmer, J. Appl. Phys. **90**, 2892 (2001).
[22] K. Shibuya, R. Dittmann, S. Mi, and R. Waser, Adv. Mater., **21**, 1 (2009).
[23] H. B. Michaelson, J. Appl. Phys. **48**, 4729 (1977).
[24] B. Psiuk, J. Szade, H. Schroeder, H. Haselier, M. Młynarczyk, R. Waser, and K. Szot, Appl. Phys. A: Mater. Sci. Process. **89**, 451 (2007).
[25] R. Oligschlaeger, R. Waser, R. Meyer, S. Karthauser, and R. Dittmann, Appl. Phys. Lett. **88**, 042901 (2006).
[26] S. Wan, R. Dittmann, U. Breuer, and R. Waser, Appl. Phys. Lett. **93**, 103109 (2008).

[27]J. H. Lee, R. Mohammedali, J. H. Han, V. Balu, S. Gopalan, C. H. Wong, and J. C. Lee, Appl. Phys. Lett. **75**, 1455 (1999).
[28]N. G. Eror, D. M. Smyth, *The Chemistry of Extended Defects in Non-Metallic Solids* (North-Holland, Amsterdam, 1970) pp. 62–74.
[29]T. Menke, P. Meuffels, R. Dittmann, K. Szot, and R. Waser, J. Appl. Phys. **105**, 066104 (2009).
[30]W. Luo, W. Duan, S. G. Louie, and M. L. Cohen, Phys. Rev. B **70**, 214109 (2004).
[31]J. R. Jameson, Y. Fukuzumi, Z. Wang, P. Griffin, K. Tsunoda, G. I. Meijer, and Y. Nishi, Appl. Phys. Lett. **91**, 112101 (2007).
[32]R. Schmiedl, V. Demuth, P. Lahnor, H. Godehardt, Y. Bodschwinna, C. Harder, L. Hammer, H. P. Strunk, M. Schulz, and K. Heinz, Appl. Phys. A: Mater. Sci. Process. **62**, 223 (1996).
[33]R. Waser, T. Baiatu, and K. H. Hardtl, J. Am. Ceram. Soc. **73**, 1654 (1990).
[34]I. Denk, W. Munch, and J. Maier, J. Am. Ceram. Soc. **78**, 3265 (1995).
[35]C. Ohly, S. Hoffmann-Eifert, X. Guo, J. Schubert, and R. Waser, J. Am. Ceram. Soc. **89**, 2845 (2006).
[36]J. Maier, *Physical Chemistry of Ionic Materials* (Wiley, West Sussex, England, 2004).
[37]R. Merkle, J. Maier, K. D. Becker, and M. Kreye, Phys. Chem. Chem. Phys. **6**, 3633 (2004).